

## **THEORY AND REALIZATION OF SIMPLE BANDPASS FILTERS WITH ANTIPARALLEL CONFIGURATION**

**Sinisa Jovanovic<sup>1, \*</sup>, Bratislav Milovanovic<sup>2</sup>,  
and Miodrag Gmitrovic<sup>2</sup>**

<sup>1</sup>IMTEL Komunikacije, Institute for Microwave Techniques and Electronics, Belgrade, Serbia

<sup>2</sup>Faculty of Electronic Engineering, University of Nis, Nis, Serbia

**Abstract**—This paper introduces a theoretical analysis as well as a design example for bandpass filters (BPF) with a distinctive topology. Based on the analysis of simple two-port symmetrical lossless networks with a parallel structure, a method for obtaining normalized BPF prototypes with desired bandwidths was developed. These prototypes can be scaled to any central frequency and symmetrical real termination in the same way as conventional filters. It is also demonstrated that with a slight modification of the basic BPF prototypes, transmission zeros with controllable frequencies can be introduced in both the lower and the upper stopband region. Such modified prototypes are more convenient for the realization of printed filters than the basic BPF prototypes. The proposed filters have almost identical characteristics in the broad vicinity of the passband region either when composed of ideal lumped elements or of transmission lines (TLs). Due to its simplicity, the proposed concept could be applied for the realization of a printed BPF at a large variety of PCB types, substrates and practical design configurations. A microstrip BPF model is realized for the experimental verification of the presented theory. The measured and theoretical results show excellent agreement, confirming the proposed concept and the exactness of the methodology.

---

*Received 28 November 2012, Accepted 5 January 2013, Scheduled 16 January 2013*

\* Corresponding author: Sinisa Jovanovic (siki@insimtel.com).

## 1. INTRODUCTION

The conventional approach to the BPF synthesis is based on one of many low-pass prototypes that have been theoretically defined in detail [1]. Then, using well-known scaling transformations, the lumped BPF elements for the desired central frequency and terminal impedances are obtained and, finally, through Richards' transformation and Kuroda's identities, so are the corresponding TLs. The main deficiency of this approach is that it often requires TLs that have high (or low) characteristic impedances whose realization is difficult or even impossible. In addition, the printed BPF obtained by this method usually occupies spacious PCB real estate that makes it unsuitable for integration. Because of these deficiencies no method provides a comprehensive and universal solution for the synthesis of BPFs with distributed parameters, especially considering all the existing technologies and substrates available for filter realization. On the other hand, a continuous development of various kinds of electronic devices and systems requires constant improvement in characteristics of RF and microwave BPFs in terms of both basic features (such as selectivity, group delay, size, weight and price) and additional attributes (such as scalability and reconfigurability). Those circumstances have stimulated the development of new types of planar filters, some of which have already been classified in textbook literature [2], while new ones are frequently published in scientific and technical journals. Most of these filters are specific, either in terms of operating frequency and width of the passband or in terms of the structure of the substrates or TL types, while a smaller number of papers propose more comprehensive solutions with a broader range of application. Some papers show that the filter's characteristics are a consequence of general network configurations, like [3] that demonstrated that the parallel connection of the two port networks has features that can be used for designing microwave BPFs, or [4] that shows that the using of a  $0^\circ$  feed structure creates two extra transmission zeros at the frequencies close to and on the opposites of the passband. A conclusion that some distinctive characteristics of the filters, such as the number and positions of the transmission and reflection zeroes, are a consequence of their topology, can be reached based on the similar characteristics of BPFs described in [5–14], distinguished by the authors into different kinds and analyzed and designed by different methods. The correlation between the topology and the electrical characteristics is especially noticeable for BPFs with capacitive coupled resonators [15–22]. The intention of this paper is to explore this correlation and to relate the electrical characteristics

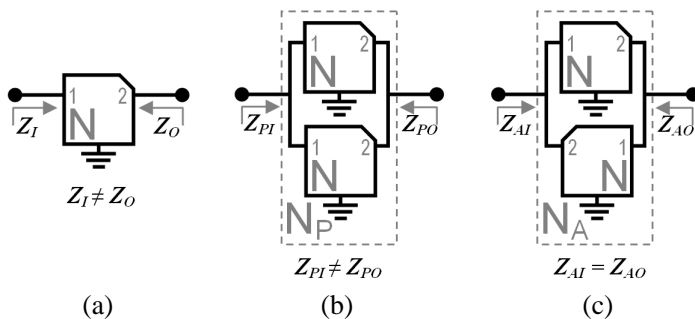


**Figure 1.** (a) basic subnetwork  $N$ . (b) Parallel connection. (c) Antiparallel connection.

of this type of filters to their distinctive topology and the component values.

## 2. ANALYSIS OF THE FILTER CIRCUIT

### 2.1. General Characteristics of an Antiparallel Configuration

The BPFs with capacitive coupled resonators share a common topology formed by a parallel connection of two identical lossless asymmetrical subnetworks  $N$  with different input and output impedances (Figure 1(a)), defined by  $ABCD$  matrix with  $A_0 \neq D_0$ :

$$\mathbf{A}_0 = \begin{bmatrix} A_0 & B_0 \\ C_0 & D_0 \end{bmatrix} \tag{1}$$

Such subnetworks can be connected in parallel in two ways:

- 1) by having mutually connected the ports with equal impedances, forming an asymmetrical resulting network, which will be referenced as a parallel connection (Figure 1(b));
- 2) by having mutually connected the ports with different impedances, forming a symmetrical resulting network, which will be referenced as an antiparallel connection (Figure 1(c)).

Since  $N$  is reciprocal, then:  $A_0 D_0 - B_0 C_0 = 1$  and therefore the  $S$  matrices for the two-port networks from Figure 1, symmetrically terminated with a real impedance  $R_0$ , can be expressed with only three  $\mathbf{A}_0$  parameters ( $A_0, C_0, D_0$ ) as applied in the following expressions:

$$N: \quad \mathbf{S}_0 = \begin{bmatrix} SN_{01}/SD_0 & SN_{02}/SD_0 \\ SN_{02}/SD_0 & SN_{01}/SD_0 \end{bmatrix}$$

$$\text{where : } \begin{cases} SN_{01} = (A_0 - R_0C_0)(D_0 + R_0C_0) - 1 \\ SN_{02} = 2R_0C_0 \\ SD_0 = (A_0 + R_0C_0)(D_0 + R_0C_0) - 1 \end{cases} \quad (2)$$

$$N_P: \mathbf{S}_P = \begin{bmatrix} SN_{P1}/SD_P & SN_{P2}/SD_P \\ SN_{P2}/SD_P & SN_{P1}/SD_P \end{bmatrix}$$

$$\text{where : } \begin{cases} SN_{P1} = (A_0 - 2R_0C_0)(D_0 + 2R_0C_0) - 1 \\ SN_{P2} = 4R_0C_0 \\ SD_P = (A_0 + 2R_0C_0)(D_0 + 2R_0C_0) - 1 \end{cases} \quad (3)$$

$$N_A: \mathbf{S}_A = \begin{bmatrix} SN_{A1}/SD_A & SN_{A2}/SD_A \\ SN_{A2}/SD_A & SN_{A1}/SD_A \end{bmatrix}$$

$$\text{where : } \begin{cases} SN_{A1} = (A_0D_0 - 1)^2 - (R_0C_0)^2 (A_0 + D_0)^2 + 4(R_0C_0)^2 \\ SN_{A2} = 4R_0C_0 (A_0D_0 - 1) \\ SD_A = ((A_0D_0 - 1) + R_0C_0(A_0 + D_0))^2 - 4(R_0C_0)^2 \end{cases} \quad (4)$$

All  $S$ -parameter numerators in (4) are either purely real or purely imaginary, which simplifies further calculations. A comparison of (2) and (3) shows that the  $S$ -parameters of the network  $N_P$  are identical to the  $S$ -parameters of subnetwork  $N$  terminated with  $2R_0$ . However, (4) shows that, under certain conditions,  $N_A$  could have significantly different  $S$ -parameters with additional transmission and reflection zeros that do not exist for  $N$  or  $N_P$ . For example, transmission zeros will exist at angular frequencies for which  $A_0D_0 - 1 = 0$  is satisfied.

### 2.2. Analysis of a Basic Antiparallel BPF

Figure 2(a) shows the simplest  $N$  that could produce  $N_A$  that has BPF characteristics and is not reducible to a ladder type filter,

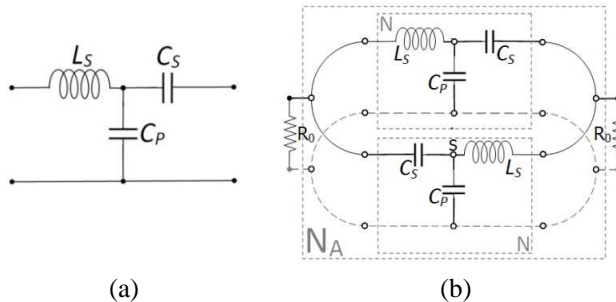


**Figure 2.** (a) The simplest configuration of subnetwork  $N$  that could form a BPF. (b) Corresponding BABPF made by the antiparallel connection of two  $N$  subnetworks.

referenced hereafter as Basic Antiparallel BPF (BABPF) and shown in Figure2(b).

For subnetwork  $N$  shown in Figure 2(a), the  $\mathbf{A}_0$  matrix becomes:

$$\mathbf{A}_0 = \begin{bmatrix} 1 - \omega^2 C_P L_S & i \cdot (\omega L_S - (1 - \omega^2 C_P L_S) (\omega C_S)^{-1}) \\ i \omega C_P & 1 + C_P C_S^{-1} \end{bmatrix} \quad (5)$$

After applying (5) in (4) with  $R_0 = 1$  and a minor rearrangement, the  $\mathbf{S}_A$  matrix for  $N_A$  becomes:

$$\mathbf{S}_A = \begin{bmatrix} SN_{A1}^*(C_S, C_P, L_S, \omega) & i \cdot SN_{A2}^*(C_S, C_P, L_S, \omega) \\ i \cdot SN_{A2}^*(C_S, C_P, L_S, \omega) & SN_{A1}^*(C_S, C_P, L_S, \omega) \end{bmatrix} / SD_A^*(C_S, C_P, L_S, \omega) \quad (6)$$

where  $SD_A^*$ , which is different from  $SD_A$  (4) due to the rearrangement, can be expressed as:

$$SD_A^*(C_S, C_P, L_S, \omega) = \begin{bmatrix} C_S C_P L_S \omega^3 - i(C_P + C_S) L_S \omega^2 - (C_P + 4C_S) \omega + i \\ C_S C_P L_S \omega^3 - i(C_P + C_S) L_S \omega^2 - C_P \omega + i \end{bmatrix} \quad (7)$$

while  $SN_{A1}^* (\neq SN_{A1})$  and  $SN_{A2}^* (\neq SN_{A2})$  are both real polynomials of  $\omega$ :

$$SN_{A1}^*(C_S, C_P, L_S, \omega) = (C_S C_P L_S)^2 \omega^6 + L_S [(C_P + C_S)^2 L_S - 2C_P C_S (C_P + 2C_S)] \omega^4 + [C_P (C_P + 4C_S) - 2L_S (C_P + C_S)] \omega^2 + 1 \quad (8)$$

$$SN_{A2}^*(C_S, C_P, L_S, \omega) = 4C_S \omega [(L_S (C_P + C_S) \omega^2 - 1)] \quad (9)$$

The  $S_{21}$  (and  $S_{12}$ ) zeros can be obtained by solving by  $\omega$  the following polynomial equation:

$$SN_{A2}^*(C_S, C_P, L_S, \omega) = 0 \quad (10)$$

that, besides  $\omega_{Z0} = 0$  gives one real and positive solution that originates from the term  $(A_0 D_0 - 1)$  and therefore doesn't exist for the subnetwork  $N$  or its parallel connection  $N_P$ :

$$\omega_{Z1} = (L_S (C_P + C_S))^{-1/2} \quad (11)$$

Angular frequencies of the  $S_{11}$  (and  $S_{22}$ ) zeros can be obtained by solving by  $\omega$ :

$$SN_{A1}^*(C_S, C_P, L_S, \omega) = 0 \quad (12)$$

Depending on the  $C_S$ ,  $C_P$  and  $L_S$  values (12) can have two ( $\omega_{p1} \neq \omega_{p2}$ ), one double ( $\omega_{p1} = \omega_{p2}$ ) or no real positive solutions, corresponding to an over-coupled, critically coupled or under-coupled filter, respectively. Since only the critical coupling is unambiguously defined, it is used as the referent condition that characterizes the filter's prototypes

normalized to  $\omega = 1$  and  $R_0 = 1$ , which is composed of normalized and dimensionless  $C_S$ ,  $C_P$  and  $L_S$  that satisfy:

$$\omega_{p1} = \omega_{p2} = 1 \quad (13)$$

Such a prototype can be scaled to obtain a filter for an arbitrary central frequency and symmetrical passive termination. The values of  $C_S$ ,  $C_P$  and  $L_S$  that satisfy (13) can be determined by simultaneously solving the following two equations:

$$SN_{A1}^*(C_S, C_P, L_S, \omega) |_{\omega=1} = 0 \quad (14)$$

$$\frac{\partial}{\partial \omega} SN_{A1}^*(C_S, C_P, L_S, \omega) |_{\omega=1} = 0 \quad (15)$$

Applying (14) and (15) on (8) gives:

$$(C_S L_S - 1)^2 (C_P^2 + 1) + C_P^2 L_S^2 - 2C_P (2C_S - L_S) (C_S L_S - 1) = 0 \quad (16)$$

$$\begin{aligned} & [(2C_S L_S - 1)^2 - (C_S^2 - 2)L_S^2] C_P^2 - 2[L_S + 4C_S^2 L_S - 2C_S(L_S^2 + 1)] C_P \\ & + 2C_S L_S (C_S L_S - 1) = 0 \end{aligned} \quad (17)$$

By setting a value for any of the three variables, for example  $C_S$ , the values of the remaining two can be calculated by simultaneously solving (16) and (17) and therefore obtaining a set of  $C_S$ ,  $C_P$  and  $L_S$  values for which (13) is satisfied, and for which the network  $N_A$  forms a BABPF prototype. One pair of real and positive values for the  $C_P$  and  $L_S$  that satisfy (16) and (17) exists for every  $C_S > 1$ . Table 1 shows such  $L_S$  and  $C_P$  values for  $C_S$  ranging from 1.5 to 100, as well as the corresponding filters' attributes: bandwidth ( $BW_{3\text{dB}}$ ), passband central frequency ( $\omega_c$ ),  $S_{21}$  zeros' frequency ( $\omega_{Z1}$ ) and frequency ( $\omega_M$ ) and  $S_{21}$  magnitude for the local minimum of isolation within the lower stopband region.

The same data is shown in Figure 3 for four sets ( $i-iv$ ) of  $C_S$ ,  $C_P$  and  $L_S$  values, illustrating that the  $N_A$  network has properties of a BPF with double  $S_{11}$  zeros at 1. The selectivity of BABPF increases with the increase of capacitances (and the decrease of inductance), so that  $BW_{3\text{dB}}$  decreases from 85.9% for  $C_S = 1.5$  to 1.4% for  $C_S = 100$  and further with the increase of  $C_S$ . A set of values ( $C_S$ ,  $C_P$ ,  $L_S$ ) that satisfy (13) exists for the infinitely high  $C_S$  so that the highest achievable selectivity of BABPF is only limited by technological constraints such are the total dielectric and conductive losses and the components' fabrication precision. The isolation in the upper stopband increases monotonically with the frequency increase as well as with the capacitor values increase. The lower stopband contains two  $S_{21}$  zeros:  $\omega_{Z0} = 0$  and  $\omega_{Z1}$  given by (11), as well as a local minimum of the isolation between them (marked with  $M^{(i)}-M^{(iv)}$ ).

**Table 1.** Components values and main characteristics for several BABPF prototypes.

	BABPFs components			main characteristics of BABPF				
	$C_S$	$C_P$	$L_S$	$BW_{3\text{ dB}}$	$\omega_c$	$\omega_{z1}$	$\omega_M$	$S_{21}(\omega_M)$
	1.5	1.1924	1.162	85.9%	1.1024	0.565	0.307	-2.5 dB
<i>i</i>	2	3.6951	0.812	75.6%	1.0684	0.465	0.144	-5.6 dB
	3	11.726	0.464	49.2%	1.0133	0.382	0.058	-9.4 dB
<i>ii</i>	4	23.737	0.321	36.2%	1.0046	0.335	0.032	-12.0 dB
	6	59.744	0.197	23.8%	1.0012	0.278	0.014	-15.5 dB
<i>iii</i>	8	111.747	0.142	17.8%	1.0005	0.243	0.008	-18.0 dB
	12	263.748	0.091	11.8%	1.0001	0.200	0.003	-21.6 dB
<i>iv</i>	16	479.749	0.067	8.8%	1+61 $\mu$	0.174	0.002	-24.1 dB
	20	759.749	0.053	7.1%	1+31 $\mu$	0.156	1.25 m	-26.0 dB
	32	1983.75	0.032	4.4%	1+7 $\mu$	0.124	0.49 m	-30.1 dB
	50	4899.75	0.020	2.8%	1+2 $\mu$	0.099	0.20 m	-34.0 dB
	64	8063.75	0.016	2.2%	1+1 $\mu$	0.088	0.12 m	-36.3 dB
	100	19799.75	0.010	1.4%	1+0.2 $\mu$	0.071	0.05 m	-40.0 dB

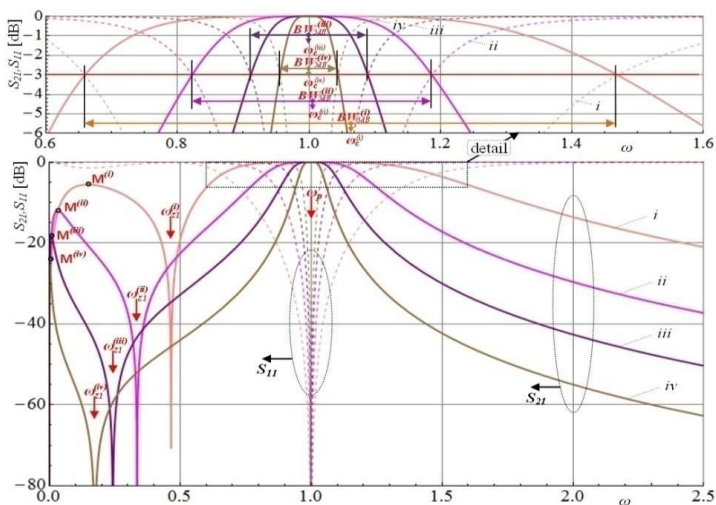


**Figure 3.**  $S$ -parameters for shaded BABPFs from Table 1.

The BABPFs with very wide passbands have poor lower stopband isolation ( $|S_{21}(\omega_M)| < 10\text{ dB}$ ) that jeopardizes their applicability. However, the isolation in the lower stopband increases for the filters with higher selectivity, while  $\omega_M$  as well as  $\omega_{z1}$  shift toward lower frequencies. Since the filter's double  $S_{11}$  zeros are, by definition, normalized to 1, the central frequency  $\omega_c$  of the passband deviates from 1. As shown in Table 1, this deviation is a few percent for the

less selective filters (10.24% for  $C_S = 1.5$  and 1.33% for  $C_S = 3$ ), while it rapidly decreases for filters with higher selectivity. If required, the less selective BABPFs can be easily scaled to align  $\omega_c$  to 1.

The characteristics of the BABPF prototype could be considered the functions of one parameter only ( $C_S$ ). A major disadvantage of such a filter is that only one of its features can be arbitrarily selected by choosing  $C_S$  (with the corresponding  $C_P$  and  $L_S$ ), while all the other characteristics have to be accepted as they are. In other words, all the filter's characteristics must be chosen as "a package", based on the most critical one. Another disadvantage is that the serial capacitance  $C_S$  is unsuitable for realization on many printed circuit substrates.

The proposed principle for generating BABPF prototypes is significant because the same concept can be applied to the analysis and enhancement of more complex antiparallel BPFs [15–22], which have been designed previously by different approximate methods and time consuming EM optimization. The BABPF prototypes are also a foundation for developing prototypes with enhanced characteristics that are more suitable for practical implementation.

### 2.3. Analysis of an Extended Antiparallel BPF

The disadvantages of the BABPF can be overcome if a filter, instead of the subnetwork from Figure 2(a), is composed of extended subnetworks, either  $N_Y$  or  $N_\Delta$ , shown in Figure 4, whose components are defined in Table 2 with two dimensionless parameters  $m$  and  $n$ , in addition to  $C_S$ ,  $C_P$  and  $L_S$  values that characterize the BABPF.

While the inductors remain the same for both  $N_Y$  and  $N_\Delta$ , the capacitors in  $N_\Delta$  are obtained from the capacitors of  $N_Y$  by the  $Y$ -to- $\Delta$  transformation. For  $m \geq 0$  and  $n \geq 0$ , all  $L$  and  $C$  values of the  $N_Y$  and  $N_\Delta$  are positive, and therefore realizable with passive components.

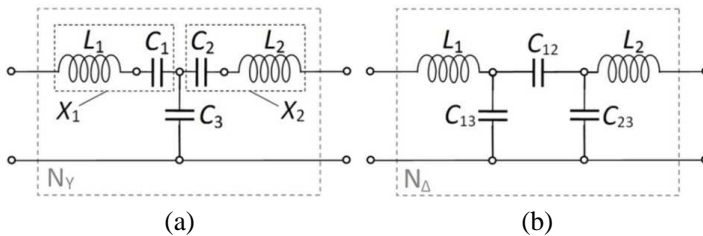


**Figure 4.** Two electrically equivalent configurations of an extended  $N$  subnetwork: (a)  $N_Y$ : with capacitors in  $Y$  configuration; (b)  $N_\Delta$ : with capacitors in  $\Delta$  configuration.

For  $L$  and  $C$  values defined according to Table 2 the admittances  $X_1$  and  $X_2$  from Figure 4(a) can be expressed as:

$$\begin{aligned} X_1 &= \omega L_1 - (\omega C_1)^{-1} = \omega(m+1)L_S - mL_S\omega^{-1} \\ &= \omega L_S + mL_S(\omega - \omega^{-1}) = X_{L_S} + mL_S(\omega - \omega^{-1}) \end{aligned} \quad (18)$$

$$\begin{aligned} X_2 &= \omega L_2 - (\omega C_2)^{-1} = n\omega C_S^{-1} - (n+1)(\omega C_S)^{-1} \\ &= -(\omega C_S)^{-1} + nC_S^{-1}(\omega - \omega^{-1}) = X_{C_S} + nC_S^{-1}(\omega - \omega^{-1}) \end{aligned} \quad (19)$$

(18) and (19) show that for  $\omega = 1$ , as well as for  $m = 0$  or  $n = 0$ , serial impedances of the extended subnetwork  $N_Y$  reduce to related serial impedances of the basic subnetwork  $N$ . They were the defining properties used to postulate the expressions listed in Table 2.

Since the subnetworks  $N_Y$  and  $N_\Delta$  are electrically equivalent, they are defined with a common  $ABCD$  matrix ( $B_E$  is not outlined because it is not used for further calculations):

$$\begin{aligned} \mathbf{A}_E &= \begin{bmatrix} A_E & B_E \\ C_E & D_E \end{bmatrix} \\ &= \begin{bmatrix} 1 - C_P L_S \omega^2 - m C_P L_S (\omega^2 - 1) & B_E(C_S, C_P, L_S, m, n, \omega) \\ i C_P \omega & 1 + C_P C_S^{-1} - n C_P C_S^{-1} (\omega^2 - 1) \end{bmatrix} \end{aligned} \quad (20)$$

By applying (20) to (4) and with minor rearrangement, an  $S$ -matrix for an Extended Antiparallel BPF (EABPF) composed of either  $N_Y$  or  $N_\Delta$  and with  $R_0 = 1$  can be obtained as:

$$\begin{aligned} \mathbf{S}_E &= \begin{bmatrix} SN_{E1}^*(C_S, C_P, L_S, m, n, \omega) & i \cdot SN_{E2}^*(C_S, C_P, L_S, m, n, \omega) \\ i \cdot SN_{E2}^*(C_S, C_P, L_S, m, n, \omega) & SN_{E1}^*(C_S, C_P, L_S, m, n, \omega) \end{bmatrix} \\ & \quad / SD_E^*(C_S, C_P, L_S, m, n, \omega) \end{aligned} \quad (21)$$

Like in (6) the numerators  $SN_{E1}^*$  and  $SN_{E2}^*$  are both real polynomials of  $\omega$ . The comparison of (20) and (5) shows that the EABPF reduces

**Table 2.** The components of  $N_Y$  and  $N_\Delta$  subnetworks as functions of  $C_S, C_P, L_S, m$  and  $n$ .

$N_Y:$	$\frac{L_1}{(m+1)L_S}$		$\frac{C_1}{1/(mL_S)}$		$\frac{C_3}{C_P}$		$\frac{C_2}{C_S/(n+1)}$		$\frac{L_2}{n/C_S}$
		↔		$Y_\Delta$		↔			
$N_\Delta:$	$\frac{L_1}{(m+1)L_S}$		$\frac{C_{13}}{(n+1)C_P/K_\Delta}$		$\frac{C_{12}}{C_S/K_\Delta}$		$\frac{C_{23}}{mC_S C_P L_S / K_\Delta}$		$\frac{L_2}{n/C_S}$
where: $K_\Delta = n+1+mL_S(C_S+(n+1)C_P)$									

to the BABPF if both  $m = 0$  and  $n = 0$ , or for  $\omega = 1$ :

$$\lim_{m \rightarrow 0 \wedge n \rightarrow 0} \mathbf{A}_E = \mathbf{A}_0 \quad \Rightarrow \quad \lim_{m \rightarrow 0 \wedge n \rightarrow 0} \mathbf{S}_E = \mathbf{S}_A \quad (22)$$

$$\mathbf{A}_E|_{\omega=1} = \mathbf{A}_0|_{\omega=1} \quad \Rightarrow \quad \mathbf{S}_E|_{\omega=1} = \mathbf{S}_A|_{\omega=1} \quad (23)$$

Analog to (11), the transfer function zeros can be calculated by solving by  $\omega$  the equation:

$$SN_{E2}^*(C_S, C_P, L_S, m, n, \omega) = 0 \quad (24)$$

The real and non-negative solutions of Equation (24) are  $\omega_{EZ0} = 0$  and two solutions given by:

$$\omega_{EZ1} = \sqrt{p_{mn} - \sqrt{p_{mn}^2 - q_{mn}}} \quad \text{and} \quad \omega_{EZ2} = \sqrt{p_{mn} + \sqrt{p_{mn}^2 - q_{mn}}} \quad (25)$$

where:  $p_{mn} = \frac{C_S}{2nC_P} + \frac{1}{2(m+1)C_P L_S} + \frac{2mn+m+n+1}{2n(m+1)}$  and

$$q_{mn} = \frac{mC_S L_S + n + 1}{n(m+1)C_P L_S} + \frac{m(n+1)}{n(m+1)}.$$

The expressions of  $m$  and  $n$  as functions of  $\omega_{EZ1}$  and  $\omega_{EZ2}$ , which are more useful for a filter design, can be obtained by solving (25) as a set of two equations for variables  $m$  and  $n$ , which gives:

$$m = \frac{1}{2} \left( \frac{\omega_{Z1}^2 - \omega_{EZ1}^2}{\omega_{EZ1}^2 - 1} + \frac{\omega_{Z1}^2 - \omega_{EZ2}^2}{\omega_{EZ2}^2 - 1} + \frac{(\omega_{Z1}^2 - 1)\sqrt{u+v}}{(\omega_{EZ1}^2 - 1)(\omega_{EZ2}^2 - 1)} \right) \quad (26)$$

$$n = 2(C_S/C_P + 1) / ((\omega_{EZ1}^2 - 1) + (\omega_{EZ2}^2 - 1) + \sqrt{u+v}) \quad (27)$$

where  $u = (\omega_{EZ1}^2 - \omega_{EZ2}^2)^2$  and  $v = 4 \frac{C_S(\omega_{EZ1}^2 - 1)(\omega_{EZ2}^2 - 1)}{C_P(\omega_{Z1}^2 - 1)}$ , while  $\omega_{Z1}$  is given by (11).

Expressions (26) and (27) give  $m$  and  $n$  values that produce transmission zeros  $\omega_{EZ1}$  and  $\omega_{EZ2}$  on arbitrary angular frequencies within the ranges:  $\omega_{Z1} \leq \omega_{EZ1} \leq 1$  and  $1 \leq \omega_{EZ2} \leq \infty$ . The ability to accurately position narrowband frequency ranges with maximum attenuation could be particularly useful for suppressing unwanted signals such as the local oscillator (LO) leakage and LO harmonics as well as the higher harmonics of the RF signal.

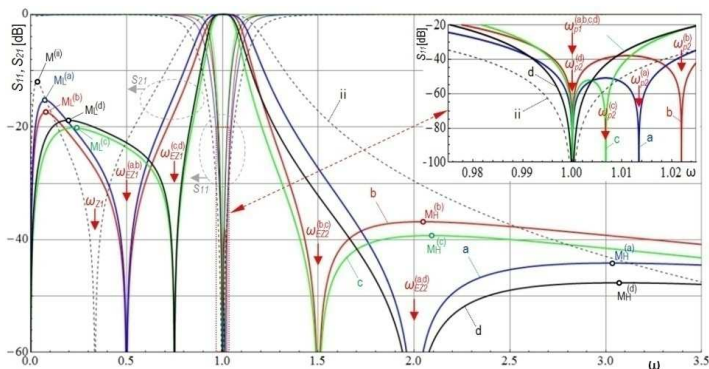
All  $L$  and  $C$  values of an EABPF composed by either  $N_Y$  or  $N_\Delta$  can be determined from Table 2 based on  $m$  and  $n$  values calculated by (26) and (27) respectively, for the specified values of  $\omega_{EZ1}$  and  $\omega_{EZ2}$ . Table 3 lists  $L$  and  $C$  values with the main characteristics for four EABPFs that have different combinations of  $\omega_{EZ1}$  and  $\omega_{EZ2}$  values, derived from the same version (*ii*) of the BABPF from Table 1, while Figure 5 compares their  $S$ -parameter frequency characteristics. It can be seen that the changing of  $\omega_{EZ1}$  and  $\omega_{EZ2}$  also affects the  $BW_{3dB}$  as well as the  $IL$  in both the upper and the lower stopband. Therefore, the characteristics of the EABPF could be more efficiently adjusted

**Table 3.** Component and parameter values and main characteristics (shaded) of four EABPF derived from the *ii* BABPF prototype from Table 1.

	$\omega_{EZ1}$	$m$	$L_1$	$C_1$	$C_3$	$C_2$	$L_2$	$n$	$\omega_{EZ2}$
a	0.5	0.178	0.378	17.47	23.737	2.875	0.098	0.391	2.0
b	0.5	0.174	0.376	17.92	23.737	2.059	0.236	0.942	1.5
c	0.75	1.017	0.647	3.064	23.737	2.062	0.235	0.940	1.5
d	0.75	1.023	0.649	3.047	23.737	2.876	0.098	0.391	2.0

	$BW_3$ dB	$S_{21}(\omega_{ML})$	$\omega_{ML}$	$C_{13}$	$C_{12}$	$C_{23}$	$S_{21}(\omega_{MH})$	$\omega_{MH}$	$\omega_c$
a	24.8%	-15.2 dB	0.076	9.409	1.140	1.548	-44.1 dB	3.031	0.9991
b	19.3%	-17.3 dB	0.079	9.732	0.844	1.118	-36.8 dB	2.047	1.0017
c	13.4%	-20.1 dB	0.222	2.520	0.219	1.696	-39.3 dB	2.092	1.0033
d	15.7%	-18.8 dB	0.195	2.438	0.296	2.302	-47.7 dB	3.070	1.0031



**Figure 5.**  $S$ -parameters comparison of EABPFs from Table 3 and the *ii* BABPF from Table 1.

against the desired filter’s specifications by changing three parameters ( $C_S, m, n$ ) instead of changing only one ( $C_S$ ) like for the BABPF.

Table 3 shows that the capacitor values can vary significantly for the EABPFs originating from the same BABPF. For  $\Delta$  configuration the sum of capacitances ranges from  $\Sigma C_{ij} = 4.435$ , for the (c) example to  $\Sigma C_{ij} = 12.097$ , for the (a) example. Those values would dominantly influence the size of the filters’ printed realization. Therefore the size comparison between the various printed filters’ designs is justifiable only if all the other filters’ characteristics are equivalent in addition to equivalent substrates,  $\omega_c$  and  $BW_3$  dB.

Like for the BABPF prototype, an EABPF prototype will have double  $S_{11}$  zeros at  $\omega = 1$  if the following two equations are

simultaneously satisfied:

$$SN_{E1}^*(C_S, C_P, L_S, m, n, \omega) |_{\omega=1} = 0 \quad (28)$$

$$\frac{\partial}{\partial \omega} SN_{E1}^*(C_S, C_P, L_S, m, n, \omega) |_{\omega=1} = 0 \quad (29)$$

As a consequence of (23), Equation (28) is identical to (16), so it will be satisfied for all solution sets  $(C_S, C_P, L_S)$  of the BABPF prototypes regardless of the  $m$  and  $n$  values. Therefore, for any  $m$  and  $n$  values, at least one  $S_{11}$  zero of the extended filter will have a unity angular frequency as can be seen in Figure 5 (detail). To achieve double  $S_{11}$  zeros at  $\omega = 1$ , the following equation derived from (29) should be satisfied simultaneously with the Equation (16):

$$k_0(C_S, C_P, L_S) + m \cdot k_m(C_S, C_P, L_S) + n \cdot k_n(C_S, C_P, L_S) = 0 \quad (30)$$

where:

$$\begin{aligned} k_0(C_S, C_P, L_S) &= C_P^2(L_S(2L_S + C_S(3C_S L_S - 4)) + 1) \\ &\quad - 2C_P(2C_S L_S - 1)(2C_S - L_S) + 2C_S L_S(C_S L_S - 1) \\ k_m(C_S, C_P, L_S) &= 2L_S(C_P^2(C_S^2 L_S - C_S + L_S) + C_P(2C_S L_S - 2C_S^2 - 1) \\ &\quad + C_S(C_S L_S - 1)) \\ k_n(C_S, C_P, L_S) &= 2(C_P^2(C_S L_S - L_S^2 - 1) - C_P(C_S(L_S^2 + 2) - 2L_S) \\ &\quad + C_S L_S - 1) \end{aligned}$$

Both Equations (16) and (30) can be satisfied in two ways:

- 1) If only one parameter (for example  $m$ ) is specified according to the required frequency  $\omega_{EZ1}$ , the other parameter (not constrained

**Table 4.** Component values and main characteristics (shaded) of the EABPF after  $C_S, C_P, L_S$  values adjustments for achieving double reflection zeros at 1.

	$\omega_{EZ1}$	$m$	$L_1$	$C_1$	$C_3$	$C_2$	$L_2$	$n$	$\omega_{EZ2}$
a	0.5	0.179	0.387	16.97	23.327	2.873	0.098	0.392	2.0
b	0.5	0.175	0.397	16.88	22.629	2.052	0.237	0.949	1.5
c	0.75	1.019	0.662	2.994	23.365	2.059	0.236	0.942	1.5
d	0.75	1.023	0.649	3.046	23.734	2.876	0.098	0.391	2.0

$Y-\Delta$

	$BW_3$ dB	$S_{21}(\omega_{ML})$	$\omega_{ML}$	$C_{13}$	$C_{12}$	$C_{23}$	$S_{21}(\omega_{MH})$	$\omega_{MH}$	$\omega_c$
a	24.9%	-15.1dB	0.077	9.169	1.129	1.552	-44.1 dB	3.031	0.9924
b	19.8%	-17.1 dB	0.083	9.190	0.833	1.117	-36.6 dB	2.055	0.9906
c	13.4%	-20.1 dB	0.225	2.462	0.217	1.693	-39.2 dB	2.094	1.0001
d	15.7%	-18.8 dB	0.194	2.438	0.295	2.302	-47.7 dB	3.070	1.0031

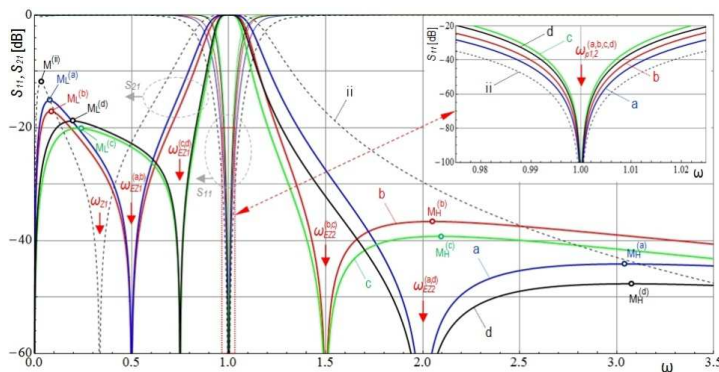


**Figure 6.**  $S$ -parameters comparison of EABPFs from Table 4 and the *ii* BABPF from Table 1.

with the filter’s specifications) can be:

$$n = -[k_0(C_S, C_P, L_S) + m \cdot k_m(C_S, C_P, L_S)] / k_n(C_S, C_P, L_S) \quad (31)$$

or, vice versa, if only  $n$  is specified according to  $\omega_{EZ2}$ , than the  $m$  value can be:

$$m = -[k_0(C_S, C_P, L_S) + n \cdot k_n(C_S, C_P, L_S)] / k_m(C_S, C_P, L_S) \quad (32)$$

- 2) If both  $\omega_{EZ1}$  and  $\omega_{EZ2}$  are specified (and therefore  $m$  and  $n$ ) like for a-d examples in Table 3, the values of  $C_S$ ,  $C_P$ , and  $L_S$  should be recalculated by simultaneously solving (16) and (30). This approach is more general than the first one, so it is used to obtain the values presented in Table 4 and in Figure 6.

The difference between the characteristics in Figures 5 and 6, as well as the components values and characteristics in Tables 3 and 4 is not significant for the most practical cases, especially if the EABPF is based on basic prototypes with a higher selectivity. However, the presented method used for calculating the component values shown in Table 4 embodies a general procedure for obtaining the EABPF prototype with double  $S_{11}$  zeros on unity angular frequency and two controllable transmission zeros, one in the lower and one in the upper stopband.

### 3. FILTER REALIZATION

#### 3.1. General Planar Topology of an EABPF

The EABPFs are suitable for fabrication in almost every technique used for filter production due to a small number of consisting elements that could easily be made with lumped elements, quasi-lumped

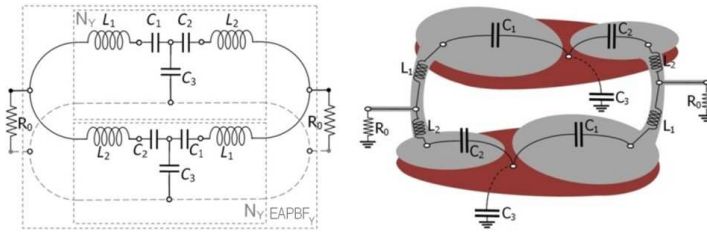


**Figure 7.** A schematic of an  $EABPF_Y$  and its general topology in the planar technique.

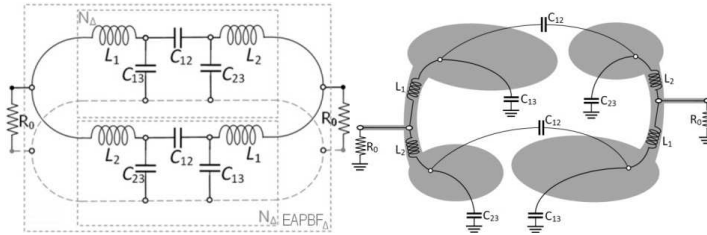


**Figure 8.** A schematic of an  $EABPF_{\Delta}$  and its general topology in the planar technique. (On both Figures 7 and 8 the ground plane is not shown for better visibility).

elements or printed TLs. Figures 7 and 8 show EABPFs made of  $N_Y$  and  $N_{\Delta}$  subnetworks, referenced as  $EABPF_Y$  and  $EABPF_{\Delta}$  respectively, together with a general topology of the filters realization in the planar technique, which tends to have a central symmetry as a consequence of the filters antiparallel configuration. The  $EABPF_{\Delta}$  is easier for fabrication because it requires only two conductive layers (one for the ground plane and one for the printed filter's layout) separated with one dielectric layer. On the other hand,  $EABPF_Y$  requires three conductive layers separated with two dielectric layers. In addition to that, as can be seen in Table 4, the total capacitance value of all the capacitors is always bigger for  $EABPF_Y$  than for the equivalent  $EABPF_{\Delta}$ . Consequently, having all other parameters equal, the printed realization of  $EABPF_Y$  will always be bigger than  $EABPF_{\Delta}$ , and therefore less suitable for fabrication in most practical cases. The only exception would be if the capacitance values required for  $EABPF_{\Delta}$  became too small for fabrication with the available technology, in which case the  $EABPF_Y$  could become a preferable option.

A multilayer substrate with a grounded top and bottom layer would be most suitable for fabrication of both EABPFs' versions. Such a substrate allows the realization of the majority of possible  $L$  and  $C$  values required for achieving specified EABPF characteristics.

### 3.2. Realization of an EABPF in the Microstrip Technique

A simple planar substrate like a microstrip (MS) could be used for fabrication of EABPF $_{\Delta}$  versions with low series  $C_{12}$  values that could be formed by edge coupling, while grounding capacitances  $C_{13}$ ,  $C_{23}$  and series inductances  $L_1$ ,  $L_2$  can be realized by TLs having low and high characteristic impedances, respectively. The electrical ( $\theta_L$ ,  $\theta_C$ ) and physical ( $l_L$ ,  $l_C$ ) lengths of inductive and capacitive MS TLs can be calculated from the following expressions derived from approximate relations for the MS TLs as well as for  $L$  and  $C$  approximation with TLs [23]:

$$\theta_L = \beta_h l_L = \frac{R_0 L}{Z_L}$$

$$\Rightarrow l_L = \frac{c_0 R_0 L}{120\pi f_c \ln(8h/w_L + w_L/4h)} \quad \text{for } w_L \leq h \quad (33)$$

$$\theta_C = \beta_l l_C = \frac{Z_C C}{R_0}$$

$$\Rightarrow l_C = \frac{60c_0 C}{\varepsilon_e f_c R_0 (w_C/h + 1.393 + 0.667 \ln(w_C/h + 1.444))} \quad \text{for } w_C \geq h \quad (34)$$

where:  $c_0$  — speed of light;  $f_c$  — central frequency;  $L$  and  $C$  — normalized element values of the prototype;  $w_L$ ,  $w_C$  and  $l_L$ ,  $l_C$  — widths and lengths of the MS TLs;  $Z_L$  and  $Z_C$  — inductive (high) and capacitive (low) characteristic impedances;  $R_0$  — termination;  $h$  — dielectric thickness;  $\varepsilon_e$  — the effective dielectric constant of a MS TL which is approximately related to the relative dielectric constant ( $\varepsilon_r$ ) as:  $\varepsilon_e = [\varepsilon_r + 1 + (\varepsilon_r - 1)(1 + 12w_C/h)^{-1/2}]/2$ .

The experimental filter model in this paper is based on the EABPF $_{\Delta}$  prototype ( $c'$ ) from Table 4 that has the values:  $L_1 = 0.661$ ,  $L_2 = 0.235$ ,  $C_{12} = 0.217$ ,  $C_{13} = 2.462$ ,  $C_{23} = 1.693$ . The components values scaled to  $f_c = 1$  GHz and  $R_0 = 50 \Omega$  are (in [nH] and [pF]):  $L'_1 = 5.265$ ,  $L'_2 = 1.875$ ,  $C'_{12} = 0.691$ ,  $C'_{13} = 7.836$ ,  $C'_{23} = 5.389$ . The model is made on the RO3010 substrate with nominal  $\varepsilon_r = 10.2$ ,  $h = 0.254$  mm and  $\tan \delta = 0.0023$ . However, based on [24] the value of  $\varepsilon_r = 11.3$  is adopted for all calculations made for the realization of the filter. The small  $h$  and high  $\varepsilon_r$  of the substrate allows a small size of MS EABPF. However, because of the constraints of the available technology, they limit the highest obtainable characteristic impedance. For the realization of the filter's inductive elements a MS TL with  $w_L = 0.11$  mm and a corresponding characteristic impedance of  $Z_L = 62.5 \Omega$  is selected, while the MS TL with  $Z_c = 50 \Omega$  has the width  $w_{50} = 0.2$  mm. Also, the initial width of  $s_g = 0.1$  mm is adopted for the gap that forms the serial capacitance  $C'_{12}$ .



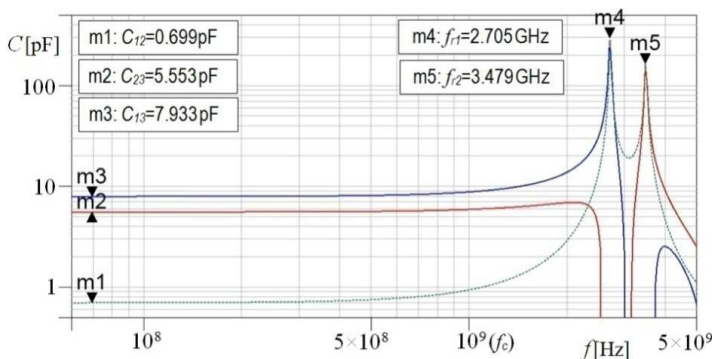


**Figure 10.** Capacitances calculated by (35) from the  $S$ -parameters of the MSCS.

used for the gap width and length optimization in order to obtain the requested  $C'_{12}$  value. Higher  $C'_{12}$  values can be reached by meandering the gap for the length increase, if its minimal thickness (determined by available technology) is reached. The results for capacitors calculated by (35) are shown in Figure 10.

The capacitance values at lower frequencies (markers m1, m2 and m3) show good agreement with the selected prototype's values, achieving relative errors of 1.28%, 3.03% and 1.23%, respectively. This validates the presented method for the MSCS dimensioning, as well as that the required  $C'_{12}$  value is very closely achieved with the initial gap dimensions. If required, the capacitors' values could be changed by scaling the corresponding parts of the MSCS layout. If the MSCS was composed only of three ideal capacitors in  $\Delta$  configuration, the capacitance values calculated by (35) would be frequency independent. The deviations from the constant values that can be seen in Figure 10 originate mostly from the serial inductances of the MSCS ( $L'_{1c}$  and  $L'_{2c}$ ), whose values can be estimated based on the capacitance values  $C'_{13}$  and  $C'_{23}$ , and resonant frequencies  $f_{r1}$  and  $f_{r2}$  (marked by m4 and m5) from the following expressions:

$$\begin{aligned} \text{scaled: } L'_{kc} &= (2\pi f_{rk})^{-2} (C'_{k3})^{-1}, \\ \text{normalized: } L_{kc} &= (f_{rk}/f_c)^{-2} (C_{k3})^{-1}, \quad \text{for } k = 1, 2 \end{aligned} \tag{36}$$

Those values should be subtracted from the prototype's inductances  $L_1$  and  $L_2$  to obtain the correct inductances for a realization with TLs whose electrical lengths at  $f_c$  are:

$$\theta_{Lk} = R_0(L_k - L_{kc})/Z_L, \quad \text{for } k = 1, 2 \tag{37}$$

The data from Figure 10 applied in (36) gives  $L_{1c} = 0.055$  and

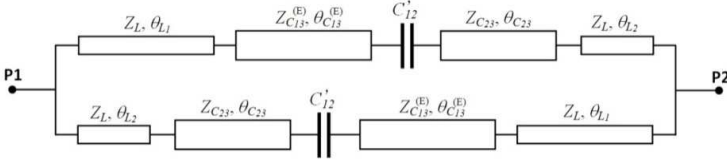


**Figure 11.** An ideal TL model for the EABPF $_{\Delta}$  ( $Z_L = 62.5 \Omega$ ,  $\theta_{L1} = 27.8^\circ$ ,  $\theta_{L2} = 8.65^\circ$ ,  $Z_{C13}^{(E)} = 7.45 \Omega$ ,  $\theta_{C13}^{(E)} = 21.03^\circ$ ,  $Z_{C23} = 11.94 \Omega$ ,  $\theta_{C23} = 23.16^\circ$ ,  $C'_{12} = 0.691 \text{ pF}$ ,  $f_c = 1 \text{ GHz}$  and  $R_0 = 50 \Omega$ ).

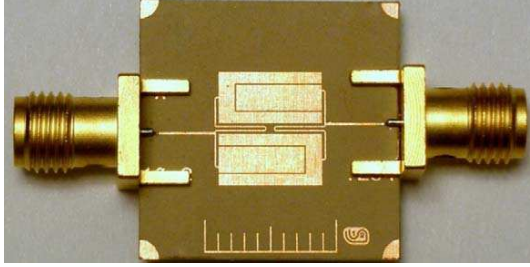


**Figure 12.** Photo of the realized microstrip EABPF $_{\Delta}$  alongside a 10 mm ruler.

$L_{2c} = 0.047$ , which applied in (37) at  $f_c = 1 \text{ GHz}$  gives the electrical lengths:  $\theta_{L1} = 0.485$  ( $27.8^\circ$ ) and  $\theta_{L2} = 0.151$  ( $8.65^\circ$ ) of inductive TLs with  $Z_L = 62.5 \Omega$ . The corresponding physical lengths (in mm) for the straight MS TLs would be (33):  $l_{L1}^{(s)} = 8.25$  and  $l_{L2}^{(s)} = 2.55$ . However, if meandered, their total physical lengths should be extended to  $l_{L1}^{(m)} = 10.56$  and  $l_{L2}^{(m)} = 2.8$  to maintain the required  $\theta_{L1}$  and  $\theta_{L2}$ .

Unlike  $C_{23}$ , the capacitance  $C_{13}$  is not realized by a simple MS TL, as can be seen in Figure 9. However, it can be modeled with an equivalent ideal TL of  $Z_{C13}^{(E)} = R_0 (L_{1c}/C_{13})^{1/2} = 7.45 \Omega$  and  $\theta_{C13}^{(E)} = (L_{1c}C_{13})^{1/2} = 0.367$  ( $21.03^\circ$ ). In this manner, all physical dimensions required for the filter MS layout shown in Figure 9 are obtained, as well as the data required for the filter's model composed of the ideal TLs and lumped series  $C'_{12}$  capacitor shown in Figure 11.

Figure 12 shows a photo of the assembled MS filter with SMA panel connectors. The filter is realized by the standard lithographic process with the line and gap width tolerances of  $\pm 5 \mu\text{m}$ . The overall filter's dimensions (excluding I/O  $50 \Omega$  lines) are  $8.52 \times 8.74 \text{ mm}$  ( $0.076\lambda_g \times 0.078\lambda_g$ , for  $f_c = 1 \text{ GHz}$  and the selected substrate). The majority of the filter's dimensions are obtained from EABPF $_{\Delta}$

prototype values by expressions given in closed form, with a limited use of EM analysis for determining the correct value of  $C'_{12}$  as well as the length of meandering MS lines.

#### 4. MEASURED RESULTS

The measured results are presented in Figure 13 and in Table 5, compared to the data obtained from the model with ideal TL lines from Figure 11, as well as with the characteristics of the corresponding EABPF $_{\Delta}$  prototype scaled to  $f_c = 1$  GHz and  $R_0 = 50 \Omega$ .

The measured results show an excellent agreement with both the prototype and the TL model. As can be seen in Figure 13, the complete frequency characteristics of the realized filter are shifted toward higher frequencies for about 3.5%. Since such a shift is not predicted by the TL model, this probably occurred because of mutual coupling of the components belonging to the filter's opposite antiparallel branches. It also caused slightly reduced isolation in the lower stopband of about 1.4 dB relative to the prototype as well as the resonance at 3.2 GHz

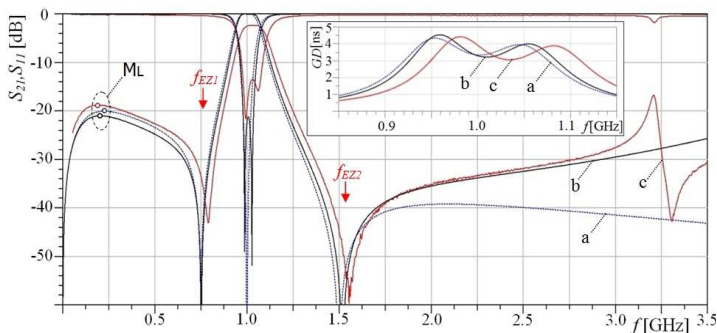


**Figure 13.**  $S$ -parameters of the example filter (**Inset** — group delay in the passband region). (a) Scaled EABPF $_{\Delta}$  prototype. (b) Filter's TL model. (c) Measured results.

**Table 5.** The main characteristics of the realized filters compared to the scaled EABPF $_{\Delta}$  prototype and the filters model composed of ideal TLs (frequencies in GHz).

	$BW_{3\text{dB}}$	$f_c$	$f_{EZ1}$	$f_{EZ2}$	$f_{ML}$	$S_{21}(\omega_{ML})$
prototype	13.39%	1.0001	0.75	1.500	0.225	-20.1 dB
TL model	13.79%	1.0081	0.75	1.519	0.204	-21.0 dB
measured	15.22%	1.0315	0.79	1.554	0.194	-18.7 dB

which was not foreseen by the TL model. Since all theoretical models were lossless they gave no prediction for  $IL$  within the passband. The  $IL$  of 2.3 dB, measured on the experimental EABPF $_{\Delta}$ , is in accordance with the typical results for bandpass microstrip filters realized on similar substrates. Both the measurement and the theory showed that the proposed filters have very slight group delay variation within the passband of less than 2 ns.

## 5. CONCLUSION

This paper introduces a detailed study of bandpass filters with antiparallel topology. It was shown that the antiparallel connection of two identical asymmetrical subnetworks could have a significantly different transfer function relative to both the single subnetwork and their parallel connection. The simplest configuration that produces a network that has the bandpass properties is identified and used for defining the BABPF prototypes with angular frequency of the double  $S_{11}$  zero normalized to unity. With a slight modification of the basic prototypes, a pair of transmission zeros can be obtained at predefined frequencies, one in the lower and one in the upper stopband region. The modified prototypes are more convenient for the practical filter realization and have improved and more assorted characteristics. The EABPF prototypes can be scaled to any desired central frequency and symmetrical termination and can be applied for the realization of a printed BPF at a variety of PCB types and substrates. The filter's elements can be realized with TLs with a wide range of characteristic impedance values. The paper outlines the efficient methodology for direct dimensioning of the required microstrip TLs based on the filter's normalized components values. An experimental microstrip filter model is made for the validation of the presented theory and methodology. The measured results show excellent agreement with the theoretical prediction of the filter's characteristics, especially considering that the experimental model is designed without full-scale EM analysis. In a future separate article the presented theory and design procedure will be extended for EABPF filters with multiple resonators.

## ACKNOWLEDGMENT

This work was partially supported by the Ministry of Education, Science and Technological Development of the Republic of Serbia under Grant TR-32052.

## REFERENCES

1. Matthaei, G. L., L. Young, and E. M. T. Jones, *Microwave Filters, Impedance Matching Networks and Coupling Structures*, McGraw Hill, 1965.
2. Hong, J. S., *Microstrip Filters for RF/Microwave Applications*, 2nd Edition, John Wiley & Sons, Inc., Hoboken, NJ, USA, 2011.
3. Osipenkov, V. and S. G. Vesnin, "Microwave filters of parallel cascade structure," *IEEE Trans. Microwave Theory Tech.*, Vol. 42, No. 7, 1360–1367, Jul. 1994.
4. Tsai, C.-M., S.-Y. Lee, and C.-C. Tsai, "Performance of a planar filter using a  $0^\circ$  feed structure," *IEEE Trans. Microwave Theory Tech.*, Vol. 50, No. 10, 2362–2367, Oct. 2002.
5. Zhu, Y.-Z. and Y.-J. Xie, "Novel microstrip bandpass filters with transmission zeros," *Progress In Electromagnetics Research*, Vol. 77, 29–41, 2007.
6. Zhang, J., J.-Z. Gu, B. Cui, and X.-W. Sun, "Compact and harmonic suppression open-loop resonator bandpass filter with tri-section SIR," *Progress In Electromagnetics Research*, Vol. 69, 93–100, 2007.
7. Dai, G. and M. Xia, "Novel miniaturized bandpass filters using spiral-shaped resonators and window feed structures," *Progress In Electromagnetics Research*, Vol. 100, 235–243, 2010.
8. Lee, S.-Y. and C.-M. Tsai, "New cross-coupled filter design using improved hairpin resonators," *IEEE Trans. Microwave Theory Tech.*, Vol. 48, No. 12, 2482–2490, Dec. 2000.
9. Namsang, A. and P. Akkaraekthalin, "A microstrip bandpass filter using asymmetrical stepped-impedance resonators," *Asia-Pacific Microwave Conference, APMC 2007*, 1–4, Dec. 11–14, 2007.
10. Kuo, J.-T. and E. Shih, "Microstrip stepped impedance resonator bandpass filter with an extended optimal rejection bandwidth," *IEEE Trans. Microwave Theory Tech.*, Vol. 51, No. 4, 1154–1159, 2003.
11. Chen, W.-N., W.-K. Chia, C.-F. Yang, and C.-L. Shih, "Improving the coupling characteristics of bandpass filters by using multilayer structure and defect ground units," *Asia-Pacific Microwave Conference, APMC 2007*, 1–3, Dec. 11–14, 2007.
12. Chu, Q.-X. and H. Wang, "Planar quasi-elliptic filters with inline EM coupled open-loop resonators," *IEEE MTT-S International Microwave Workshop Series on Art of Miniaturizing RF and Microwave Passive Components*, 47–50, Dec. 2008.

13. Krongkitsiri, W., C. Mahatthanajatuphat, and P. Akkaraekthalin, "Wideband bandpass filters using parallel-coupled sirs with wide spurious suppression," *Progress In Electromagnetics Research C*, Vol. 27, 69–83, 2012.
14. Lee, K. C., H. T. Su, and M. K. Haldar, "Compact microstrip bandpass filters using triple-mode resonator," *Progress In Electromagnetics Research Letters*, Vol. 35, 89–98, 2012.
15. Jovanovic, S. and A. Nestic, "Microstrip bandpass filter with new type of capacitive coupled resonators," *Electronics Letters*, Vol. 41, No. 1, 19–21, Jan. 2005.
16. Jovanovic, S. and A. Nestic, "Printed band-pass filter at L band," *14th IST Mobile & Wireless Communications Summit*, Dresden, Jun. 19–23, 2005.
17. Jovanovic, S. and A. Nestic, "A new microstrip bandpass filter for UHF range," *7th TELSIKS 2005*, Vol. 1, 167–169, Niš, Serbia, Sep. 28–30, 2005.
18. Jovanovic, S. and A. Nestic, "New filter type suitable for miniature printed bandpass filters at RF & microwave frequencies," *European Microwave Conference*, 25–28, Paris, Oct. 3–7, 2005.
19. Jovanovic, S. and A. Nestic, "Capacitive coupled microstrip bandpass filter with asymmetrically capacitive loaded resonators," *Mediterranean Microwave Symposium MMS 2007*, 113–116, Budapest, Hungary, May 14–16, 2007.
20. Prabhu, S., J. S. Mandeep, and S. Jovanovic, "Microstrip bandpass filter at S band using capacitive coupled resonator," *Progress In Electromagnetics Research*, Vol. 76, 223–228, 2007.
21. Mandeep, J. S., S. Prabhu, and S. Jovanovic, "Design of capacitive coupled resonator microstrip filter," *Microwave and Optical Technology Letters*, Vol. 50, No. 2, 460–462, Feb. 2008.
22. Jovanovic, S., "An overview of microwave bandpass filters with capacitive coupled resonator," *Microwave Review*, Vol. 16, No. 2, Dec. 2010.
23. Pozar, D. M., *Microwave Engineering*, 4th Edition, John Wiley&Sons, New York, 2011.
24. Rautio, J. C., "Measurement of uniaxial anisotropy in Rogers RO3010 substrate material," *IEEE International Conference on Microwaves, Communications, Antennas and Electronics Systems, COMCAS 2009*, 1–4, Nov. 9–11, 2009.